JOURNAL OF MATERIALS SCIENCE 25 (1990) 4075–4079

Phase fields in rapidly solidified MnTi and MnAlTi alloys studied by X-ray diffraction

A. R. YAVARI, J. L. VERGER-GAUGRY
LTPCM-CNRS UA 29, Institut National Polytechnique de Grenoble, BP 75, 38402 Saint Martin d'Hères, France

While rapid solidification causes little modification of phase fields in Mn_xTi_{1-x} alloys for $x <$ 30 at %, alloys richer in manganese present metastable phases. A structure intermediate between crystalline and quasi-crystalline phases is observed in the range $0.3 < x < 0.45$. Aluminium addition is found to stabilize the C14 phase down to manganese contents as low as 35 at % and $Mn_{35}(AlTi)_{65}$ is found to be single-phased C14. The ternary alloy's C14 phase field emerges due to aluminium substitution for manganese at low manganese contents.

1. Introduction

On the titanium-rich side of the MnTi phase diagram (see Fig. 1), the high temperature bcc β-Ti exhibits a maximum manganese solubility $x_{Mn} < 30$ at % while hexagonal β-Ti at lower temperatures shows little manganese solubility [1]. Near $x_{Mn} = 0.5$, intermetallic MnTi (tetragonal, ϕ, together with the ρ phase of undetermined crystal structure [1]) with complicated crystalline structures appears and at higher manganese contents the C14-$MgZn_2$ type Mn_2Ti hexagonal laves phase forms. We examine these phase fields in microcrystalline MnTi alloys obtained by rapid solidification. Waterstrat *et al.* [2] studied the Mn_2Ti-C14 phase. Both the a and c lattice parameters of this hexagonal phase were found to expand with addition of the larger titanium atoms above 33 at % and the phase was found to be stable up to the composition $Mn_{55}Ti_{45}$. It was shown that this stability was due to partial occupation of manganese-type sites by titanium atoms. The stability of the C14 structure on the manganese-rich side is interrupted by the formation of Mn_3Ti. We have also examined the effect of aluminium addition on the Mn_2Ti Laves phase stability. To our knowledge, terniary MnAlTi phase diagrams covering the composition range of the C14 phase have not yet been reported. It was found that addition of aluminium allows further substitution for manganese such that a single-phased hexagonal C14 structure with as low as 35 at % Mn is obtained. Aluminium addition thus stabilizes the Laves phase.

2. Experimental procedure

MnTi and MnAlTi alloys of various compositions were prepared by induction melting in a cold crucible and in alumina crucibles, respectively, and under argon gas. The ternary alloys were of compositions $Mn_x(Al_{51}Ti_{49})_{1-x}$ hereafter referred to as $Mn_x(AlTi)_{1-x}$. The Al/Ti ratio was varied for a few more compositions to map out the C14 phase-field as indicated later in Fig. 6. The alloys were melt-spun on a copper substrate at speeds up to 80 m sec^{-1}. Most of the ribbons were 30 to 50 μm thick. They were brittle and broke into small pieces upon collision with the quench-chamber walls. The entire chamber was evacuated to 10^{-5} torr and then refilled with pure helium gas for the quenching experiments. X-ray diffraction patterns were obtained on the as-quenched samples and after annealing for 2 h at 800° C (1073 K) in sealed quartz tubes under purified argon gas. A Siemens diffractometer was used with copper $K\alpha$ radiation ($\lambda = 0.154$ nm).

3. Results

Fig. 1 shows the TiMn phase diagram. Pure titanium with hcp structure transforms the bcc structure at $T < 900$° C (1173 K). However, β-Ti containing manganese can be easily retained by quenching down to room temperature. Fig. 2 shows X-ray diffraction spectra for various rapidly solidified MnTi alloys. Pure titanium exhibits only hcp peaks (Fig. 2a) and MnTi with $x_{Mn} = 15$ at % predominantly hcp peaks (Fig. 2b) together with smaller β-Ti peaks. We note that the (1 1 0) peak of β-Ti is superimposed on the (0 0 1) hcp peak. At 20 at % Mn (Fig. 2c), hcp peaks have disappeared and only β-Ti peaks are observed. This is consistent with the phase diagram of Fig. 1

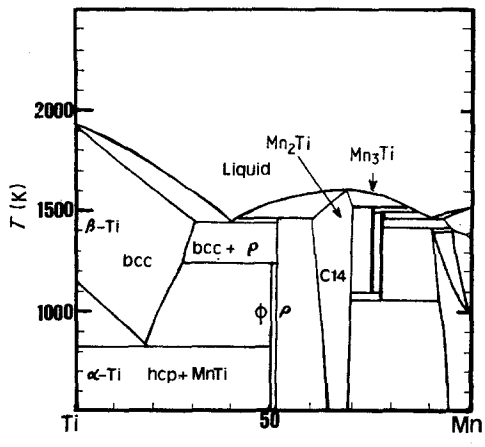

Figure 1 Mn–Ti phase diagram as reconstructed by Murray [1].

0022–2461/90 $03.00 + .12

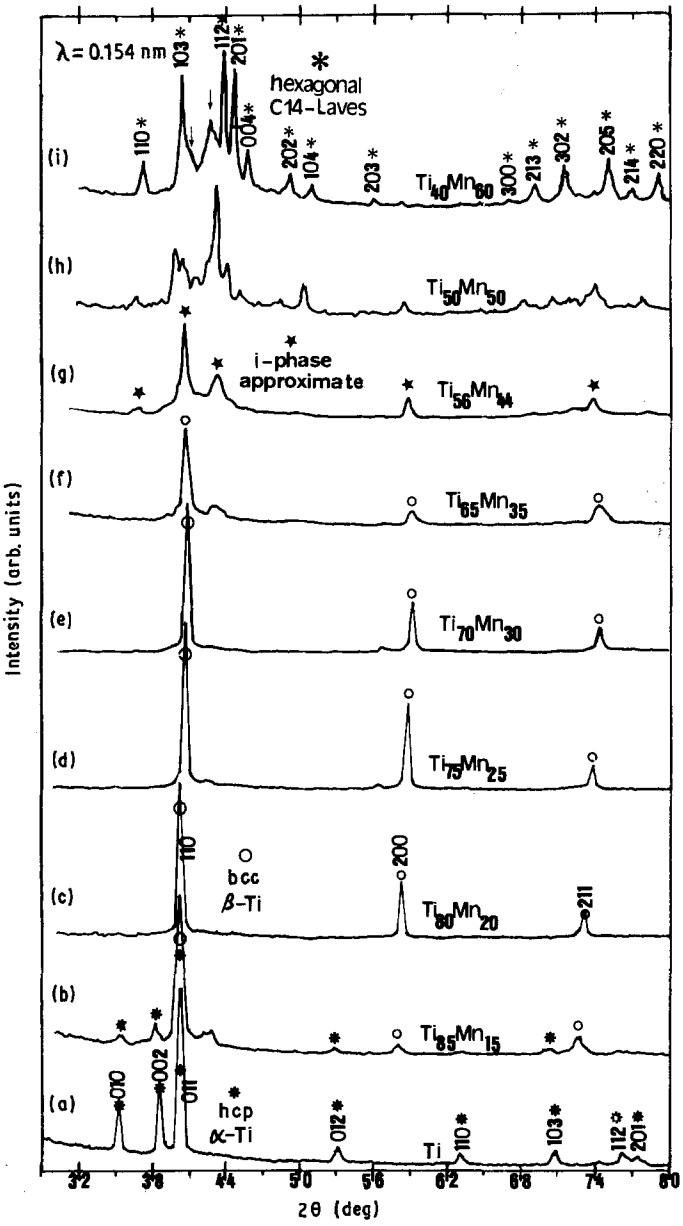

Figure 2 X-ray diffraction patterns for rapidly solidified Mn_xTi_{1-x} alloys in the range $0 < x < 60$ at.% (Cu$K\alpha$ radiation).

which shows that for $x_{Mn} > 20$ at %, the stable phases at $T > 600°C$ are β-Ti and MnTi (ϕ or ρ). It also shows that at temperatures below the β-Ti phase field, complicated intermetallic phases do not nucleate as easily as hcp α-Ti observed in the sample with $x_{Mn} = 0.15$ at %. Figs 2d and e show that for $x_{Mn} = 25$ and 30 at %, respectively, β-Ti is again retained. With increasing manganese content, the β-Ti peaks are displaced towards higher angles. The alloy with $x_{Mn} = 0.30$ should contain some intermetallic MnTi but no such peaks appear. This indicates that solid solubility of Mn in bcc titanium is enhanced by rapid solidification.

At the composition $30 \leqslant x_{Mn} \leqslant 50$ at %, X-ray spectra should normally show increasing predominance of peaks due to intermetallic MnTi (ϕ and possibly ρ). However, in this composition range, diffraction continues to occur at the angles corresponding to β-Ti peaks, but these peaks are drastically broadened (Figs 2f and g). Furthermore, a fourth and even broader peak appears near the (1 1 0) β-Ti peak and a weak one at lower angles as can be seen in Fig. 2g. These diffraction peaks, which can be fitted with good approximation to an AlMn-type icosahedral quasi-crystalline (qc) lattice [3] are, in fact, due to one of its approximate periodic structures [3, 4].

The Bragg peaks of the rapidly solidified $Mn_{50}Ti_{50}$ (Fig. 2h) can be indexed to the tetragonal ϕ phases although they are significantly broadened. All but one of the major Bragg peaks of the $Mn_{60}Ti_{40}$ alloy (Fig. 2i) can be indexed to those of the Mn_2Ti-C14 hexagonal Laves phase.

Fig. 3 shows the spectra for these samples before and after annealing for 2 h at 800° C (1073 K). As expected, annealed $Mn_{60}Ti_{40}$ shows only Mn_2Ti-C14 peaks. The unidentified broad peak at $2\theta = 42.8°$ and the shoulder at $2\theta = 41°$ (see arrows in Fig. 3c) have disappeared after annealing thus indicating that they belong to a metastable phase which has not yet been identified although the peak positions are close to those of the major peaks of the qc approximate periodic structure of Fig. 3e. $Mn_{50}Ti_{50}$ after annealing shows a much more developed ϕ-phase pattern (Fig. 3h). All other compositions in the range $0.30 < x_{Mn} < 0.50$ show both ϕ-phase and β-Ti peaks after annealing as expected from the phase diagram isotherms at 800° C. Interestingly, the intermetallic phase peaks also begin to emerge in samples with $0.15 < x_{Mn} < 30$ at %

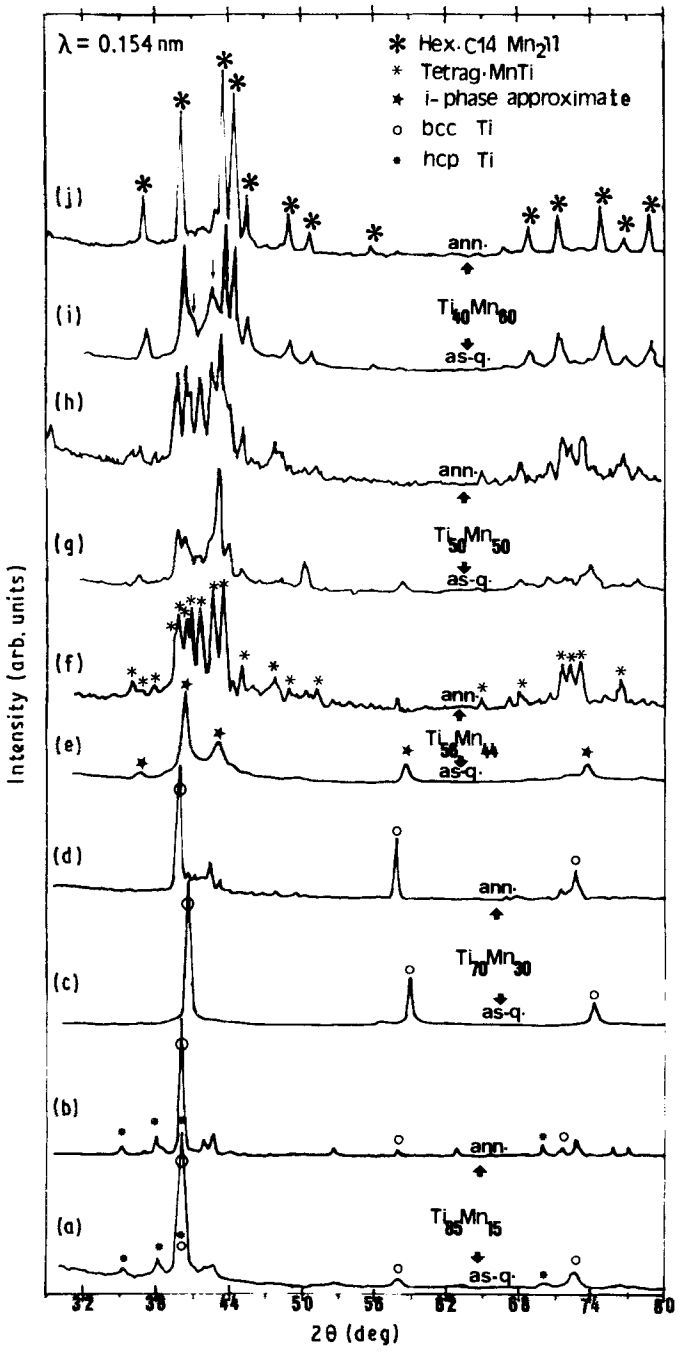

Figure 3 X-ray diffraction patterns for rapidly solidified Mn_xTi_{1-x} alloys in as-quenched (as-q) and annealed (ann) states.

after annealing even though the annealing temperature places the composition range in the β-Ti phase-field. Apparently the slow cooling upon removal from the furnace allows sufficient time for significant phase separation.

In a preliminary report on the structure of some microcrystalline MnAlTi alloys [3], we reported an X-ray pattern for rapidly solidified $Mn_{35}(AlTi)_{65}$. Subsequent identification revealed, somewhat unexpectedly, that the spectrum could be fully indexed by the C14 hexagonal symmetry of the Mn_2Ti Laves phase. Because MnAlTi ternary phase diagrams are unavailable, we have further examined the structures of rapidly quenched $Mn_{55}(AlTi)_{45}$ and $Mn_{20}(AlTi)_{80}$ alloys before and after annealing at 800° C (1073 K). The X-ray diffraction patterns obtained for these samples are shown in Fig. 4. Of the three alloys only Mn_{35} $(AlTi)_{65}$ is single-phased hexagonal C14 in its as-quenched and annealed states. The manganese-poor and manganese-rich alloys both present significant extra peaks that are modified after annealing. From the Bragg peak intensities of as-quenched $Mn_{20}(AlTi)_{80}$, it would appear that it is constituted of the C14 Laves phase up to a volume fraction more than 50%. The extra peaks due to an unidentified metastable phase give way after annealing to those of the tetragonal $L1_0$ AuCu-type ordered AlTi (Figs 4d and e) while the C14 Laves peaks become less intense. $Mn_{55}(AlTi)_{45}$ also consists mostly of Mn_2Ti-C14 phase with one major and a few minor unidentifed peaks indicated by arrows in Fig. 4f, which become more important after annealing but remain less intense than those of the C14 phase. The few available peaks of this minority phase have not yet allowed crystallographic identification. However, the same X-ray peaks appear in the slowly cooled ingot and a secondary electron micrograph of a section of this ingot shows large and small grains of C14 phase together with an important

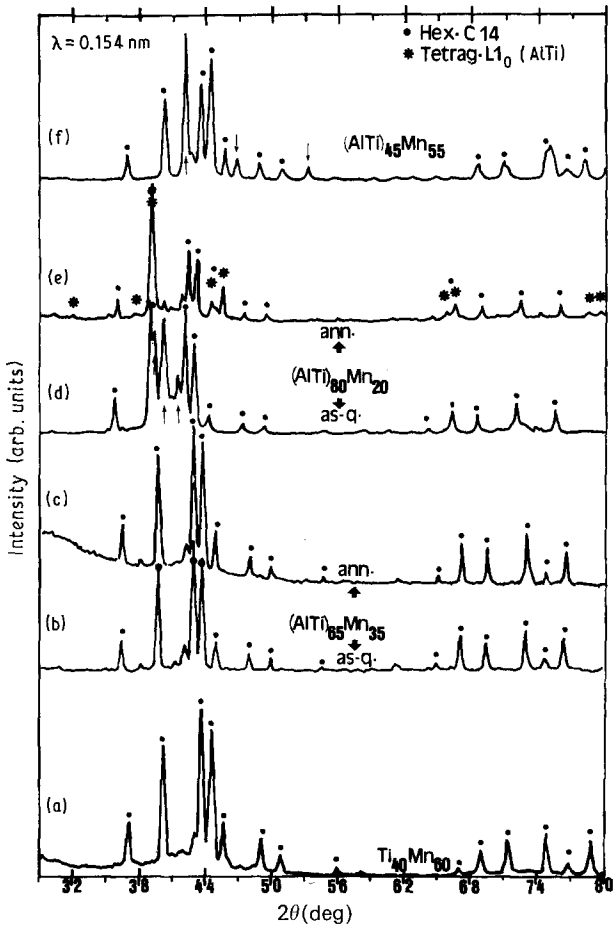

Figure 4 X-ray diffraction patterns for rapidly solidified $Mn_x(AlTi)_{1-x}$ alloys in as-quenched (as-q) and annealed (ann) states.

number of black areas (Fig. 5) which energy dispersive X-ray microanalysis indicated to be very rich in aluminium. Thus both $Mn_{20}(AlTi)_{80}$ and $Mn_{55}(AlTi)_{45}$ are constituted of more than 50 vol % C14 while the $Mn_{35}(AlTi)_{65}$ alloy is fully hexagonal C14. Furthermore, $Mn_{35}(AlTi)_{65}$ remained in the fully C14 phase after annealing. Further examination showed that even in ingot form, it presented a nearly identical X-ray spectrum that was fully indexed by C14 Bragg peaks. These results do not prove that the C14 phase is the equilibrium structure for $Mn_{35}(AlTi)_{65}$ but indicate that if it is a metastable phase, it is a very stable one. In any case, it can be concluded that the Mn_2Ti-type C14 Laves phase appears in a wide composition range of the ternary MnAlTi alloys and a

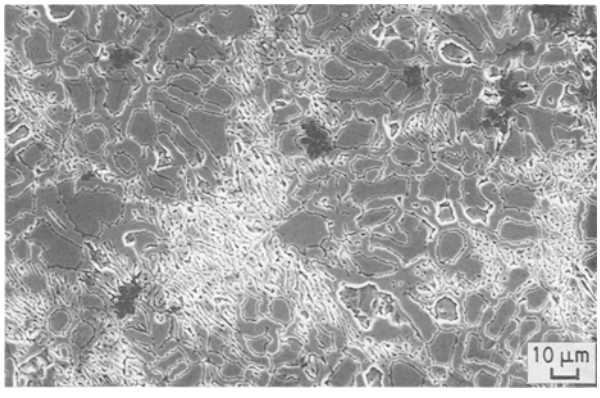

Figure 5 Secondary electron micrograph of $Mn_{55}(AlTi)_{45}$ ingot showing aluminium-rich minority black phase.

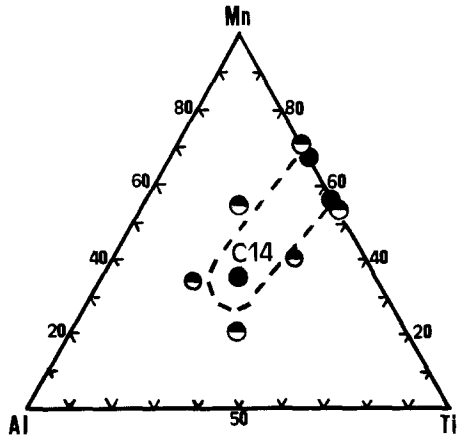

Figure 6 Schematic MnAlTi phase diagrams showing tentative map of C14 phase field: (○) fully C14; (◓) partially C14.

corresponding metastable phase diagram is traced in Fig. 6.

4. Discussion

Titanium-rich rapidly quenched Mn–Ti alloys exhibit phase fields and microstructures that are predictable from the phase diagram. The high-temperature bcc β-Ti, which is stable up to x_{Mn} just below 30 at % at about 1400 K (see Fig. 1), is easily quenched down to room temperature. While in the rapidly quenched alloy with $x_{Mn} = 0.3$ only bcc Bragg peaks appear, at higher manganese contents these peaks are strongly broadened and new peaks begin to appear (Fig. 2). Prior to this composition range and due to the size difference between titanium and manganese alloys, the lattice parameter of bcc titanium decreases rapidly with manganese addition. It can be seen in Fig. 7 that $d(1\,1\,0)$ drops linearly with x_{Mn} up to 30 at % and begins to increase in the range $0.3 < x_{Mn} < 0.35$ which is consistent with the appearance of extra Bragg peaks belonging to a new phase in this range (Fig. 2). The lattice parameter a_0 of pure bcc titanium at 900° C (1173 K) is 0.3306 nm. Using a coefficient of thermal contraction, $\alpha = 2 \times 10^{-5}\,K^{-1}$, one obtains for the hypothetical bcc titanium at room temperature, $a_0 = 0.3240$ nm and $d(1\,1\,0) = a_0/2^{1/2} = 0.2290$ nm.

This value is plotted as an open circle on the vertical axis of Fig. 7 and it can be seen to fall on the linear fit of d (1 1 0) against x_{Mn} up to 30 at %. This line corresponds to the simple relation

$$d(1\,1\,0) = \frac{22^{1/2}}{3}(x_{Mn}r_{Mn} + x_{Ti}r_{Ti}) \qquad (1)$$

which yields $r_{Mn} = 0.1232$ nm and $r_{Ti} = 0.1402$ nm in as-quenched β-Ti compared with room-temperature values $r_{Mn} = 0.135$ nm and $r_{Ti} = 0.147$ nm for cubic manganese and hcp titanium, respectively. These differences imply a negative mixing volume of about 0.5 $cm^3\,mol^{-1}$ or 5.2% for the $Mn_{30}Ti_{70}$ solid solution.

The phase diagram indicates that the alloys in the range $0.3 < x_{Mn} < 0.5$ should exhibit a mixed structure of β-Ti and intermetallic MnTi tetragonal ϕ (or ρ) phases. However, the rapidly solidified alloys in the range $0.35 < x_{Mn} < 0.45$ at % show a strong broadening of the bcc peaks and the emergence of additional broad peaks which can together be indexed

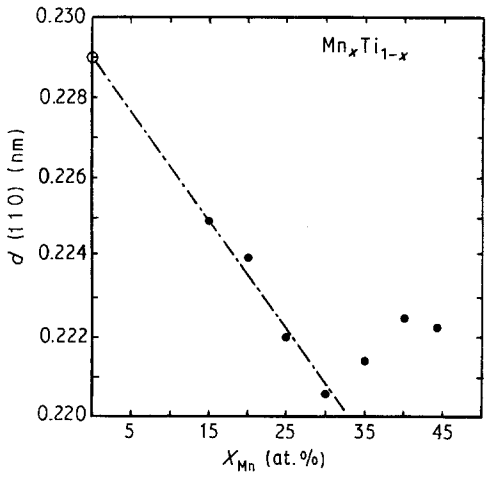

Figure 7 $d(1\,1\,0)$ interplanar spacing plotted against manganese content in bcc (β-Ti) Mn_xTi_{1-x} solidified alloys.

with an i-phase quasi-crystalline symmetry with the low-angle i-phase peaks being absent. Some electron diffraction patterns (EDP) show bright spots with five- or ten-fold symmetry superimposed on a periodic network [3]. Dong *et al.* [4] have recently provided clear examples of such five- or ten-fold electron diffraction patterns superimposed on periodic networks in some EDPs of rapidly solidified $FeTi_2$ and $Ni(TiV)_2$ whose corresponding Frank–Kasper type phases are predominantly built of icosahedral structural units. It appears that our alloys exhibit related structures [3] in the range between MnTi and $MnTi_2$ and this is not surprising as icosahedral motifs are also predominant in the tetragonal MnTi and C14 Mn_2Ti Laves phases. Fig. 3f shows how, upon annealing, this metastable phase transforms into the MnTi ϕ-phase together with residual β-Ti. Such metastable phases may also be responsible for the unidentified Bragg peaks appearing in the spectrum for the rapidly solidified $Mn_{60}Ti_{40}$ (see arrows in Fig. 3i) which disappear after annealing. This point will be further investigated by TEM.

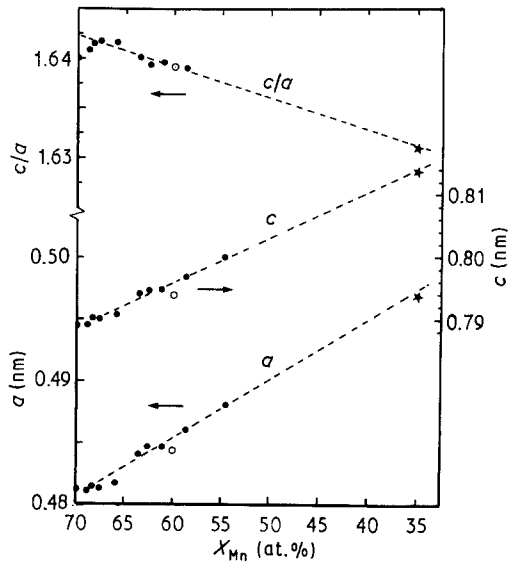

Figure 8 Hexagonal C14 lattice parameters plotted against manganese content in Mn_xTi_{1-x} alloy (●) [2], (○) present work, and $Mn_x(AlTi)_{1-x}$ (*) present.

The results of our investigation of the C14 phase field in ternary AlMnTi alloys revealed that compositions as poor in manganese as $Mn_{35}(AlTi)_{65}$ form a single-phase C14 Laves phase upon solidification. This was somewhat unexpected as Waterstrat *et al.* [2] had previously shown that the stability of the Mn_2Ti-C14 phase is limited to compositions with $x_{Mn} \geqslant 55$ at %. Fig. 8 shows a and c lattice parameters of the hexagonal C14 phase as a function of x_{Mn} as extracted from their results, and on which we have plotted our own values obtained from the diffraction patterns of $Mn_{60}Ti_{40}$ and $Mn_{35}(AlTi)_{65}$ using $a = 2d(1\,1\,0)$ and $c = 4d(0\,0\,4)$ of Figs 2 and 3. It can be seen that a and c and c/a for the ternary alloy fall nicely on the extrapolation of the lattice parameter of the binary MnTi alloys towards lower manganese content. Because Waterstrat *et al.* [2] have shown that the observed evolution of the lattice parameters is due to titanium substitution in manganese sites, it is concluded that in ternary $Mn_{35}(AlTi)_{65}$, aluminium substitutes and compensates for manganese, thus rendering the C14 phase stable down to at least 35 at % Mn. The good linear fit of Fig. 8 is consistent with the nearly equal atomic diameters of titanium and aluminium atoms. While the C14 stable phase field has not been completely traced out in ternary MnAlTi alloys, a metastable phase diagram is presented in Fig. 6.

Icosahedral qc phases have been observed in $NiTi_2$ [5] and $FeTi_2$ [6], and, as discussed earlier, MnTi alloys in the composition range between $MnTi_2$ and MnTi show structures that are intermediate between quasi-crystalline and crystalline phases [3]. These observations together with the ease of formation of qc structures in aluminium-rich AlMn alloys could lead to the expectation that ternary alloys may form quasi-crystals near the composition $Mn_{35}(AlTi)_{65}$. It was seen, however, that this composition range massive substitution of manganese by aluminium allows easy nucleation and growth of the C14 phase whose formation must be suppressed to favour quasi-crystalline growth during solidification.

References

1. J. L. MURRAY, *Bull. Alloy Phase Diag.* **2** (1981) 334.
2. R. M. WATERSTRAT, B. N. DAS and P. A. BECK, *Trans. Metall. Soc. AIME* **224** (1962) 512.
3. A. R. YAVARI and J. L. VERGER-GAUGRY, *J. Mater. Sci.* **23** (1988) 3383.
4. D. S. ZHOU, H. Q. YE, D. W. LI and K. H. KUO, *Phys. Rev. Lett.* **60** (1988) 2180.
5. Z. ZHANG, H. Q. YE and K. H. KUO, *Phil. Mag.* **51** (1985) L49.
6. C. DONG, Z. K. HEI, L. B. WANG, Q. H. SONG, Y. K. WU and K. H. KUO, *Scripta Metall.* **20** (1986) 1155.

Received 4 May
and accepted 29 September 1989